A Simple Method with Analytical Model to Extract Heterojunction Solar Cell Series Resistance Components and to Extract the A-Si:H(i/p) to Transparent Conductive Oxide Contact Resistivity

Er-Chien Wang[1, a)], Anna B. Morales-Vilches[1], Sebastian Neubert[1], Alexandros Cruz[1], Rutger Schlatmann[1] and Bernd Stannowski[1]

[1]*Helmholtz-Zentrum Berlin, PVcomB, Schwarzschildstr. 3, 12489 Berlin, Germany*

[a)] Corresponding author: er-chien.wang@helmholtz-berlin.de

Abstract. Silicon heterojunction (SHJ) solar cell technology has the potential to be the next mainstream industrial solar cell design due to its high efficiency and lean production process with only four main process steps. While two-side contacted SHJ cells have very high open circuit voltages (V_{oc}) >740 mV, they tend to be lower in short circuit current density (J_{sc}) and fill factor (*FF*). Understanding the series resistance (R_s) components of such cells is crucial as these cells have two extra TCO/a-Si/Si contact resistances due to the optically absorptive passivating electrodes. Reducing the R_s components contribution is essential to improve the *FF*. In this paper, we report a straightforward and simple analytical model to break down the R_s of our SHJ solar cell having >23% efficiency into its components with the aid from common characterization methods, namely transfer length method (TLM) and Cox and Strack method. We derived the silicon bulk to transparent conductive oxide (TCO) contact resistivity through the amorphous-silicon (a-Si:H) intrinsic/p-doped stacks, a parameter that is not measureable directly, from experimental SHJ solar cell results, using front-junction, rear-junction and front finger number variation setups. We found it to be 0.30 ± 0.07 Ωcm^2. Further reducing this value is one of the keys to improve SHJ solar cell's *FF*.

INTRODUCTION

Silicon heterojunction solar cell technology has proven to achieve outstanding conversion efficiency and is a potential candidate in large-volume manufacturing due to its lean production procedures [1]. In a conventional SHJ front and rear contacted solar cell, the crystalline silicon wafer is passivated and contacted on both sides by hydrogenated amorphous silicon (a-Si:H) intrinsic/n-doped and intrinsic/p-doped stacks as electron and hole collectors, respectively. These passivated contact schemes can achieve excellent passivation and large volume manufacturing potential due to only four main process steps: wet chemistry for saw-damage removal and surface texturing, plasma-enhanced chemical vapor deposition (PECVD) intrinsic/doped a-Si:H deposition, transparent conductive oxide (TCO) sputtering and screen-printing metallization, while fully processed at low temperature (<220°C).

For SHJ solar cells, due to the low conductivity of the doped a-Si:H contact layers, TCO layers are necessary for lateral carrier transport towards the metal grid electrode and providing good ohmic contact between the TCO and metal fingers [2]. The TCO on the front side of the cell also serves as antireflection coating (ARC), whereas, the TCO on the rear side can be part of the rear reflector structure. Optimizing the TCO layers, especially the front TCO, is mainly a trade-off between short-circuit current (J_{sc}) and fill-factor (*FF*) or, more specifically on the material property side, between transparency and lateral conductivity. The effect of passivation degradation due to TCO deposition damaging the a-Si:H layer underneath and other possible degradations should also be considered.

Understanding the series resistance (R_s) contribution within SHJ solar cells is crucial as optimizing both V_{oc} and J_{sc} involves a trade-off with R_s, especially since SHJ cell design has two extra contact resistances when compared to conventional c-Si cells due to the optically absorptive a-Si:H passivating electrodes. Lachenal et al. have reported a method to breakdown the R_s of a 6 inch SHJ cell, however, it is missing the silicon bulk contribution in lateral conductance under illumination and at the same time resistance through the silicon bulk thickness [3].

In this paper, we demonstrate a simple analytical model to calculate the R_s components within a completed solar cell without the use of simulation tools for carrier distributions. We then apply the model to a few different cell structures to verify the model with experimental results. However, please note that the different cell structures are not designed for efficiency optimization but R_s variation. Finally, we can obtain the R_s contribution and hence the contact resistivity of TCO through a-Si:H(i/p) stacks to silicon bulk, which is not directly measureable due to the p-n junction.

R_S COMPONENTS CALCULATION

When determining the R_s of solar cells, it is essential to identify the two types of R_s associated with either current path under illumination ($R_{s,light}$) or without illumination ($R_{s,dark}$) [4]. There are three resistive contacts on each side of the wafer that are partially contributing to the total $R_{s,light}$ of a SHJ solar cell. The first resistive contact is the work function mismatch between the silicon bulk and a-Si:H carrier selective contacts (larger bandgap than silicon bulk), which may create energetic barriers for the carriers. The second resistive contact is the work function mismatch between a-Si:H carrier selective contacts and TCO layer, which can form an opposing diode. The third resistive contact is the TCO layer to metal fingers contact, which also introduces carrier transport resistances. The first two barriers specifically have great impact on the solar cell's V_{oc}, J_{sc} and FF as the doping and thickness of the a-Si:H layer are restricted. This is because even though a-Si:H layer has excellent passivation capability, the a-Si:H layer itself is a good optical absorber in the short wavelength range and the resistance through the layer also increases with increasing thickness. A thick a-Si:H layer will reduces the J_{sc} significantly when applied to the front of the solar cell and also increase the total R_s when applied to either the front or the back of the solar cell. Other contributions to the R_s includes the silicon bulk lateral and vertical resistance as well as lateral resistance within front and rear TCO and front and rear metal grid electrodes. Bivour et al., and Cruz et al., both have demonstrated that by switching from front emitter to rear emitter design, the lateral conductivity of the front TCO can be coupled into the silicon bulk absorber, where the lateral resistance calculation requires parallel resistors model for layers with parallel carrier flow [5,6].

There are a few ways to determine the $R_{s,light}$ as summarized by Pysch et.al., where illumination intensity variation method, Suns-V_{oc} and one-sun current-voltage (IV) curve comparison method and the light-dark IV comparison with $R_{s,dark}$ correction method are all determined to be reliable and robust [7]. The advantage of the light-dark IV method adopted in this paper is that the R_s information can be obtained from just a single IV measurement setup with a shutter system. On the other hand, the illumination intensity variation method normally requires lamp stabilization time, which prolongs the measurement time. However, it is important to note that the principle of superposition required for the light-dark IV method to work is only valid when the SHJ solar cell IV curve has no "S-shape" feature, i.e. has good FF (>77%) [8].

To determine the R_s components of a SHJ solar cell, we first extract the total R_s of the cell at maximum power point (MPP) by using the light-dark IV comparison method proposed by Aberle et al. and correction proposed by Dicker [9,10]. The first part of equation (1) describes the voltage difference at the maximum power point under one-sun condition and dark condition. The second part of equation (1) describes the voltage drop due to $R_{s,dark}$, where $R_{s,dark}$ can be described by equation (2).

$$R_{S,light\_dark,corr.} = \frac{V_{dark,mpp} - V_{light,mpp}}{|J_{light,mpp}|} - \frac{(|J_{SC}| - |J_{light,mpp}|)R_{S,dark}}{|J_{light,mpp}|} \quad (1)$$

$$R_{S,dark} = \frac{V_{dark,J_{SC}} - V_{OC}}{|J_{SC}|} \quad (2)$$

Figure 1 below plots the light IV and J_{sc} shifted dark IV. The components of equation (1) and (2) can be found in figure 1.

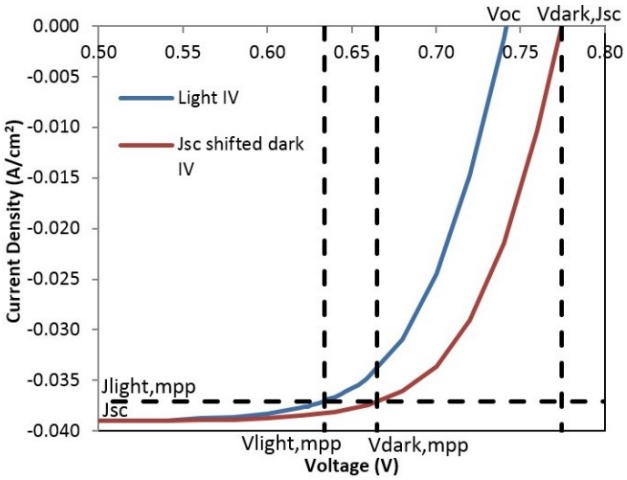

FIGURE 1. Light IV and J_{sc} shifted dark IV.

In order to calculate the bulk lateral conductance contribution, we need to know the bulk resistivity under one-sun illumination. The V_{mpp} and J_{mpp} mentioned below are all under light condition and R_s is the $R_{s,light\_dark,corr}$. We first calculate the R_s free V_{mpp} from equation (3) and then from equation (4) calculate the Δn at MPP as shown by Adachi et al., which is the minority carrier concentration at R_s free V_{mpp} [11].

$$V_{mpp(R_{s\_free})}(J_{mpp}) = V_{mpp}(J_{mpp}) + J_{mpp}R_{S,light\_dark,corr}(J_{mpp}) \tag{3}$$

$$\Delta n(mpp) = \sqrt{\left(\frac{N_d+N_a}{2}\right)^2 + {n_i}^2 exp\left(\frac{qV_{mpp(R_{s\_free})}}{k_B T}\right)} - \frac{N_d+N_a}{2} \tag{4}$$

In equation (4), N_d and N_a are the donor and acceptor concentrations respectively, n_i is the intrinsic carrier concentration, q is the electron charge, k_B is the Boltzmann constant and T is the absolute temperature. Equation (5) below describes the resistivity of the silicon bulk in terms of the corresponding carrier types, assuming all dopants are fully ionized. Based on the silicon bulk base doping type, concentration and law of mass action (the product of free electrons and holes concentration is equal to the intrinsic carrier concentration squared under thermal equilibrium), it is possible to calculate the corresponding electron and hole concentration within the bulk under illumination. Along with Klaassen's mobility ($\mu_{n,p}$) model with fit improvement mentioned in PVlighthouse, it is now possible to calculate the bulk resistivity ($\rho_{n,p}$) in terms of either electron or holes under one-sun illumination [12,13].

$$\rho_{n,p} = \frac{1}{q*\mu_{n,p}*(n,p+\Delta n,\Delta p)} \tag{5}$$

Equation (6) below shows the bulk contribution to the lateral conductance of both the front and rear TCO. Depending on the p-n junction position, the majority and minority current flow are very different. For a front p-n junction bifacial cell design, assuming all photogenerations exist near the front surface, the front surface lateral R_s contribution can be calculated from TCO $R_{sheet,front}$ in parallel with $R_{sheet,bulk,minority}$, where $R_{sheet,bulk,minority}$ can be obtained by $\rho_{bulk,minority}$ dividing by the wafer thickness. The rear surface lateral R_s contribution is then TCO $R_{sheet,rear}$ in parallel with $R_{sheet,bulk,majority}$. The R_s contribution from $R_{sheet,lateral}$ for both front and rear can then be calculated similarly to the emitter sheet resistance contribution to R_s of a homojunction cell. The R_s contribution from carriers travelling through the wafer thickness is calculated with equation (7) below, where the $\rho_{bulk,vertical}$ in this case is the bulk majority carrier resistivity. For a rear p-n junction bifacial cell design, the bulk majority carrier now is responsible for front lateral conductivity, and minority carrier is responsible for rear lateral conductivity and conductivity through the wafer thickness. For monofacial design, it is simpler as the rear metal sheet dominates rear lateral conductivity.

$$R_{sheet,lateral} = \left(\frac{1}{R_{sheet,TCO}} + \frac{1}{R_{sheet,bulk,\,lateral}}\right)^{-1} \tag{6}$$

$$R_{vertical} = \rho_{bulk,vertical} * W \quad (7)$$

The metal grid R_s contribution can be estimated by analytical modeling proposed by Fellmeth et al., and the metal to TCO contact resistance can be found using the transfer length method (TLM) approach [14]. The lumped contact resistivity from silicon bulk through the a-Si:H(i/n) layer to the TCO layer can be obtained from Cox and Strack method or TLM method [15]. Lastly, the lumped contact resistance from silicon bulk through the a-Si:H(i/p) layer to TCO that cannot be directly measured due to the p-n junction, however, can be obtained from removing all other contributions from the cell total R_s.

EXPERIMENT SETUP

To fabricate the SHJ solar cells, we prepare ten 2 x 2 cm² cells on each 5 inch n-type Czochralski (CZ) 5 Ωcm silicon wafer. The wafers are first saw-damage etched and textured in KOH solutions resulting in 125 μm thick wafers. Later, after RCA cleaning finishing with 1% concentration HF dip to deglaze, intrinsic and n-type/p-type a-Si:H are deposited on both sides of the wafer by plasma enhanced chemical vapor deposition (PECVD) with AKT1600 cluster tool from Applied Materials. Indium tin oxide layers (ITO) are deposited through aligned masks defining the cell area on both sides of the wafer as front and rear TCOs with an in-line DC sputtering system from Leybold Optics. Silver grids are created on both sides of the wafer by screen-printing with low temperature paste from Namics Corporation. Lastly, the completed cells are characterized using a current voltage (*J-V*) measuring system WXS-155S-L2 dual source class AAA+ sun simulator from Wacom under dark and AM1.5G standard test conditions with 2 x 2 cm² shadow masks. More detailed fabrication procedures can be found elsewhere [16].

EXPERIMENTAL RESULTS

To test the model, six wafers with ten cells on each wafer have been fabricated. All cells have the same i/n amorphous/nano-crystalline silicon layers stack, i/p amorphous silicon layers stack and the same sputtered ITO based i/n side TCO with a sheet resistance of 110 Ω/□ and i/p side TCO of around 80 Ω/□. TLM structures are also included on the same wafers to ensure close-to-cell TCO/metal characterizations. The variations from wafer to wafer are the junction side (front vs. rear) and the number of fingers on the front. Wafer 7 and 8 are the exact same wafer as wafer 5 and 6 but flipped up-side-down, however, in this paper they will be treated like separate wafers. The metallization contact fraction for 12 fingers is 4.3% and the metallization fraction for 25 fingers is 9.6%. It should be noted that only wafer 1 and 2 are structurally optimized, wafer 3 and onwards are structural variations to purposely vary the R_s. Table 1 below summarizes the cell structures with the best and the averaged cell *J-V* parameters. From the table, it can be seen that front-junction cell structure typically has slightly lower J_{sc} compared to the rear-junction counterpart. The reason for the lower J_{sc} is due to the parasitically absorptive a-Si:H(p) layer on the front, which was originally optimized for the rear only. For wafer 5 to 8 the much lowered J_{sc} is due to the increased number of metal fingers on the front causing greater optical shading and ultimately lowering the V_{oc} as V_{oc} is depended on the light-generated current.

TABLE 1. Cell structures and J-V parameters of the best cell and average over ten cells

Wafer number:	Cell structure	V_{oc} (mV) best/average	J_{sc} (mA/cm²) best/average	FF (%) best/average	η (%) best/average
1 and 2	Rear-junction, 12 fingers front and 25 fingers rear	741/739 741/739	38.6/38.6 38.6/38.5	81.6/79.9 81.4/79.9	23.4/22.7 23.3/22.7
3 and 4	Front-junction, 12 fingers front and 25 fingers rear	739/738 737/736	37.1/36.9 36.7/36.6	81.4/80.7 81.1/80.3	22.3/22.0 21.9/21.6
5 and 6	Rear-junction, 25 fingers front and 25 fingers rear	737/735 736/734	34.4/34.2 34.3/34.3	82.0/80.8 81.8/80.7	20.8/20.3 20.7/20.3
7 and 8	Front-junction, wafer 5 and 6 but flipped upside down	735/733 735/733	33.5/33.5 33.8/33.5	82.3/80.9 81.9/80.8	20.3/19.9 20.3/19.9

Over the 8 wafers with ten solar cells on each wafer, both V_{oc} and J_{sc} within the same wafer have small difference between the best and the averaged values, which means the deviation is small. The largest contribution to the efficiency deviation from the best cell results to averaged cell results within the same wafer comes from the fill factor. Comparing different wafers but same structure shows similar V_{oc}, J_{sc} and FF, where the FF still has the largest deviation from best cell results to averaged cell results. A breakdown of the light and dark IV method extracted R_s values are summarized in table 2 below, where the shaded values are the lumped contact resistance from silicon bulk through the a-Si:H(i/p) layer to the TCO layer obtained by removing all other contributions from the cell total R_s. Please note that the contact resistance from metal fingers to TCO is small (<0.005 Ωcm^2) and hence not reported in the table.

TABLE 2. R_s components break down in Ωcm^2 (the shaded values are calculated from R_s total minus all other contributions)

Wafer number:	Front metal grid	Front TCO	Front TCO/ bulk	Si bulk	Rear TCO/ bulk	Rear TCO	Rear metal grid	Total (Ωcm^2)
1	0.21	0.12	0.06	0.06	0.27	0.03	0.09	0.84
2	0.21	0.12	0.06	0.06	0.37	0.03	0.09	0.94
3	0.21	0.15	0.29	0.02	0.06	0.03	0.09	0.83
4	0.21	0.15	0.24	0.02	0.06	0.03	0.09	0.78
5	0.09	0.03	0.06	0.07	0.34	0.03	0.09	0.70
6	0.09	0.03	0.06	0.07	0.28	0.03	0.09	0.65
7	0.09	0.03	0.33	0.02	0.06	0.03	0.09	0.65
8	0.09	0.03	0.31	0.02	0.06	0.03	0.09	0.62

Figure 2 (a) below plots the boxplot of R_s of all cells on each wafer in green and the averaged R_s of all ten cells with open squares. The remaining R_s contribution from lumped contact resistance from silicon bulk to TCO through the a-Si:H(i/p) stacks are plotted with filled squares and values shown in shaded cells in table 2, and is averaged to all cell structures to be 0.30 ± 0.07 Ωcm^2. This is the same value for contact resistivity as the contacting area equals to the total cell area. Figure 2 (b) plots the averaged cell R_s breakdown from wafer one. Agreeing with results shown by Lachenal et al., the contact resistance from silicon bulk to TCO through a-Si:H(i/p) stacks contributed the largest portion of R_s (slightly below one third in our case), whereas, front metal grid comes second at 25% for our cells [3].

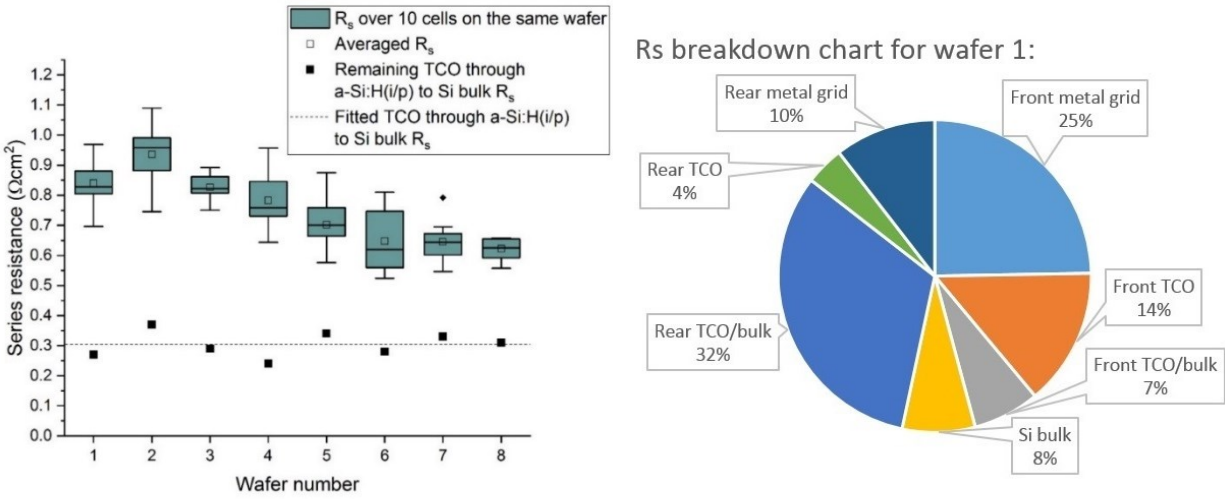

(a) (b)

FIGURE 2. (a) The total R_s of different cell structures and the remaining contact resistance from the silicon bulk to TCO through the a-Si:H(i/p) stacks; (b) The averaged cell R_s breakdown pie chart for wafer one.

CONCLUSION

In conclusion, this paper demonstrates a simple method with analytical model to extract heterojunction solar cell series resistance components and to extract the silicon bulk through a-Si:H(i/p) to TCO contact resistivity. Firstly, the R_s of the solar cell is extracted from illuminated and dark IV measurements or any other well-known methods from literature. From the R_s free V_{mpp}, the minority carrier injection level can be calculated and hence silicon bulk resistivity under illumination. The TCO sheet resistance measured with TLM method coupled with silicon bulk gives the lateral series resistance contribution from the TCO. The contact resistivity from silicon bulk through a-Si:H(i/n) to TCO can be measured with Cox and Strack method, whereas the finger and busbar resistances can be calculated from existing analytical models. Lastly, the contact resistivity from silicon bulk through a-Si:H(i/p) to TCO can be approximated from removing all other contributions. By varying the junction location, front and rear TCO sheet resistance and the number of fingers on the front, the contact resistivity through a-Si:H(i/p) is averaged to be $0.30 \pm 0.07\ \Omega cm^2$, which contributes to roughly one third of the total series resistance. Future work to reduce the contact resistivity includes introducing a more heavily doped a-Si:H(p) layer and or different crystalline structure for the layer. As for the TCO layer, it is also possible to lower the contact resistivity through higher work function TCOs or reducing ITO doping for better work function alignment for carrier transport.

ACKNOWLEDGMENTS

We would like to thank the co-workers at HZB for their support on the solar cell fabrication: Matthias Zelt and Tobias Henschel for PECVD depositions, Katja Mayer-Stillrich and Manuel Hartig for sputtering depositions, Holger Rhein for screen-printing metallization and Stefan Janke for characterization. This work was financially supported by the German Ministry of Economic Affairs and Energy (BMWi) under contract no. 0324189C within the project "ProSelect" and "Dynasto" project under contract no. 0324293B.

REFERENCES

1. K. Yamamoto, K. Yoshikawa, H. Uzu, and D. Adachi, Jpn. J. Appl. Phys. **57**, 08RB20 (2018).
2. S. De Wolf, A. Descoeudres, Z. C. Holman, and C. Ballif, Green **2**, 7-24 (2012).
3. D. Lachenal, D. Baetzner, W. Frammelsberger, B. Legradic, J. Meixenberger, P. Papet, B. Strahm, and G. Wahli, Energy Procedia **92**, 932-938 (2016).
4. L. D. Nielsen, IEEE Trans. on Electron Devices ED- 29, 821-827 (1982).
5. M. Bivour, S. Schröer, M. Hermle, S. W. Glunz, Sol. Energy Mater. Sol. Cells **122**, 120-129 (2014).
6. A. Cruz, E. –C. Wang, A. B. Morales-Vilches, D. Meza, S. Neubert, B. Szyszka, R. Schlatmann, and B. Stannowski, Sol. Energy Mater. Sol. Cells **195**, 339-345 (2019).
7. D. Pysch, A. Mette, and S. W. Glunz, Sol. Energy Mater. Sol. Cells **91**, 1698-1706 (2007).
8. U. Das, S. Hegedus, L. Zhang, J. Appel, J. Rand, and R. Birkmire, "Investigation of hetero-interface and junction properties in silicon heterojunction solar cells", Proceedings of the 35th IEEE Photovoltaic Specialists Conference, Honolulu, Hawaii, USA, 2010, pp. 1358-1362.
9. A. G. Aberle, S. R. Wenham, and M. A. Green, "A new method of accurate measurements of the lumped series resistance of solar cells", Proceedings of the 23rd IEEE Photovoltaic Specialists Conference, Louisville, Kentucky, USA, 1993, pp. 133-139.
10. J. Dicker, "Analyse und Simulation von hocheffizienten Silizium-Solarzellenstrukturen für industrielle Fertigungstechniken" Ph.D. thesis, University of Konstanz, 2003.
11. D. Adachi, J. L. Hernández, and K. Yamamoto, Appl. Phys. Lett. **107**, 233506 (2015).
12. D. B. M. Klaassen, Solid-State Electron. **35** (7), 953-959 (1992).
13. www.pvlighthouse.com.au
14. T. Fellmeth, F. Clement, and D. Biro, IEEE J. Photovolt. **4** (1), 504-513 (2014).
15. R. H. Cox, and H. Strack, Solid-State Electron. **10**, 1213-1218 (1967).
16. A. B. Morales-Vilches, A. Cruz, S. Pingel, S. Neubert, L. Mazzarella, D. Meza, L. Korte, R. Schlatmann, and B. Stannowski, IEEE J. Photovolt. **9**, 34-39 (2019).